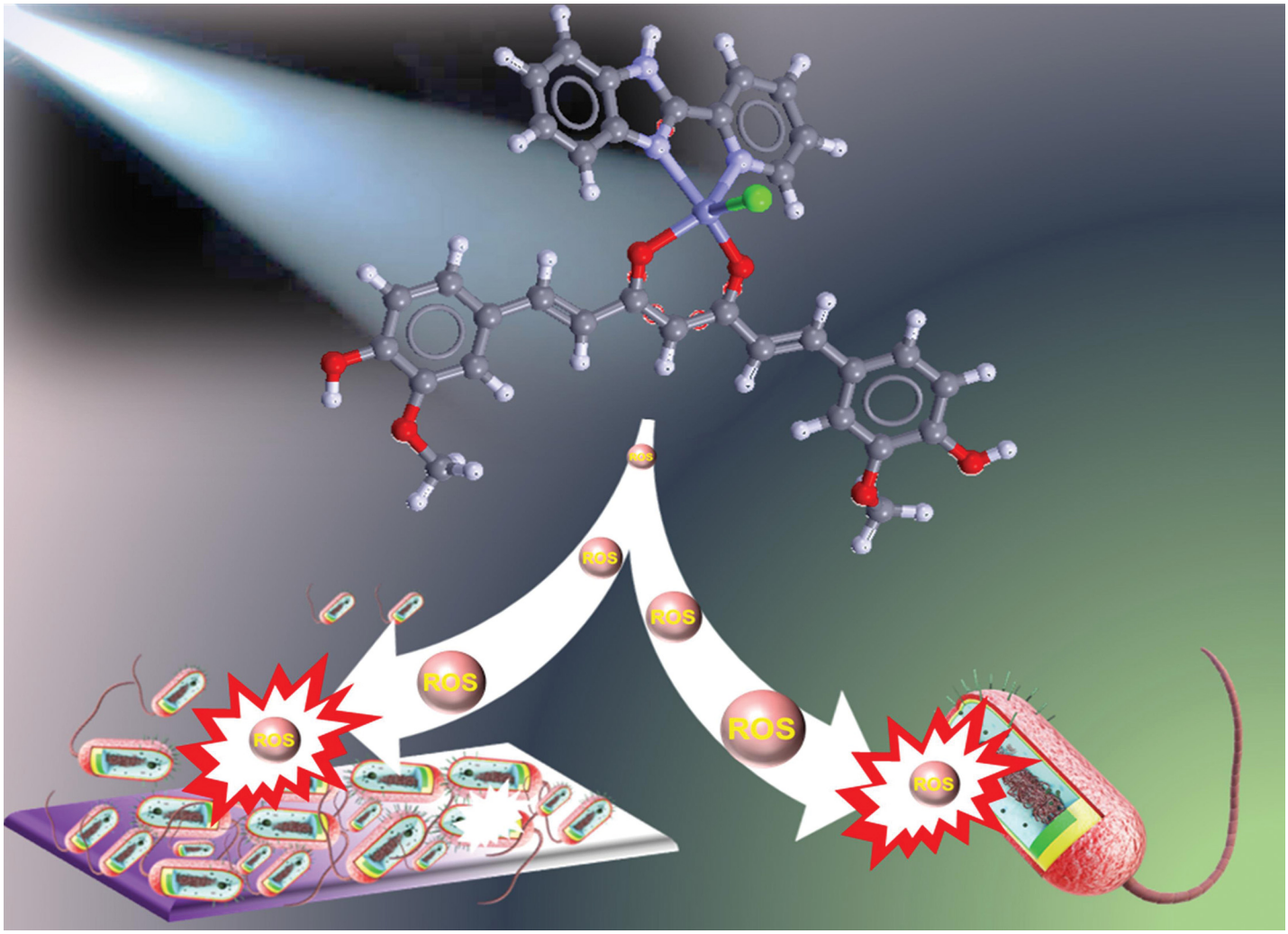

Showcasing research from Dr Samya Banerjee's and Dr Sudip Mukherjee's Laboratories, Department of Chemistry and School of Biomedical Engineering, Indian Institute of Technology (BHU), Varanasi, Uttar Pradesh 221005, India

Zn(II)-metallo-photoantibiotics: experimental and computational approach identifying a therapeutic role for antibacterial and antibiofilm applications

Curcumin-derived Zn(II)-metallo-photoantibiotics demonstrated effective antibacterial and antibiofilm activities against *E. coli* and *B. subtilis*. Computational studies revealed that these photoantibiotics can generate ROS and interact with bacterial proteins. *In vitro* and *in vivo* findings underscored their efficacy for aPDT applications.

Image reproduced by permission of Sudip Mukherjee, *Chem. Commun.*, 2025, **61**, 10307.

As featured in:

See Sudip Mukherjee, Samya Banerjee *et al.*, *Chem. Commun.*, 2025, **61**, 10307.

ROYAL SOCIETY OF CHEMISTRY

rsc.li/chemcomm

Registered charity number: 207890

ChemComm

COMMUNICATION

View Article Online
View Journal | View Issue

Cite this: *Chem. Commun.*, 2025, **61**, 10307

Received 26th April 2025,
Accepted 9th June 2025

DOI: 10.1039/d5cc02340h

rsc.li/chemcomm

Zn(II)-metallo-photoantibiotics: experimental and computational approach identifying a therapeutic role for antibacterial and antibiofilm applications†

Rajesh Kushwaha, ‡[a] Sangeeta Kumari,‡[b] Arya Mishra,[a] Anjali Upadhyay,[b] Archana Rai,[c] Malay Nayak,[b] Sudip Mukherjee *[b] and Samya Banerjee *[a]

The antibacterial profiles of curcumin-based novel Zn(II)-metallo-photoantibiotics against *E. coli* and *B. subtilis* are reported. *In silico* studies indicated their ROS generation capacity and binding interaction with bacterial proteins. Therapeutic results indicated the advantages of these Zn(II)-metallo-photoantibiotics in antibacterial photodynamic therapy.

Antimicrobial resistance (AMR) is one of this century's most pressing global health challenges.[1] Current antibiotics, predominantly based on organic molecules, are increasingly failing due to the rapid evolution of resistant bacterial strains.[2,3] Traditional approaches, including clinical antibiotic modification or developing new organic compounds, often fail due to their single-target mechanisms.[2,3] Henceforth, researchers have been investigating next-generation antibiotics and novel antibacterial therapies to tackle these challenges. Recently, antibacterial photodynamic therapy (aPDT) has shown great potential to overcome drug resistance problems due to its different mechanisms of action.[4,5] Due to the multi-targeting ability of the generated ROS, aPDT can potentially damage a wide range of bacterial strains regardless of their drug resistance.[4,5] Also, developing resistance to aPDT is unlikely due to shorter drug-light interaction, minimal dark toxicity, extensive cellular damage preventing cross-generational adaptation, *etc.*[5,6] Moreover, aPDT selectively targets bacterial infection sites without harming healthy tissues.[5,6] Recently, metal complexes have caught attention as antibacterial agents. The Community for Open Antimicrobial Drug Discovery recently reported that metal complexes have outstanding hit rates (10×) against critical bacteria compared to organic molecules and can overcome the AMR problem.[3,7] Therefore, various transition metal complexes, including Ir(III), Ru(II), Os(II), Pt(II), and Re(I), have caught significant attention as promising aPDT agents.[5,7] However, concerns about the inherent toxicity of heavy metals have prompted a shift toward exploring 3d metal-based alternatives.[8] Among 3d metals, zinc is essential, required for several physiological and intracellular biochemical functions.[9] Although Zn(II) is highly biocompatible and shows strong antibacterial potential with phthalocyanine- and porphyrins, Zn(II) complexes remain scarcely explored for aPDT applications.[10] Herein, we developed novel photo-responsive Zn(II) complexes, [Zn(cur)(pybi)Cl] (**Zn1**), [Zn(cur)(Me-pybi)Cl] (**Zn2**), and [Zn(cur)(pen-pybi)Cl] (**Zn3**), where acac = acetyleacetonate; cur = curcumin anion; pybi = 2-(pyridin-2-yl)-1*H*-benzo[*d*]imidazole; Me-pybi = 1-methyl-2-(pyridin-2-yl)-1*H*-benzo[*d*]imidazole; pen-pybi = 1-pentyl-2-(pyridin-2-yl)-1*H*-benzo[*d*]imidazole (Fig. 1a) aimed at harnessing visible light for antibacterial therapy. Curcumin has been utilized due to visible light absorption/emission properties and its ability to produce ROS upon light irradiation, causing oxidative stress and damaging bacterial components.[11] Benzimidazole has been used for its well-established antimicrobial properties.[12] The alkyl substitutions at the benzimidazole moiety were strategically introduced to modulate lipophilicity and photophysical behavior.[12]

Zn1–Zn3 were synthesized (Scheme S1, ESI†) and characterized thoroughly (Fig. S1–S10, ESI†). HPLC analysis of **Zn1–Zn3**

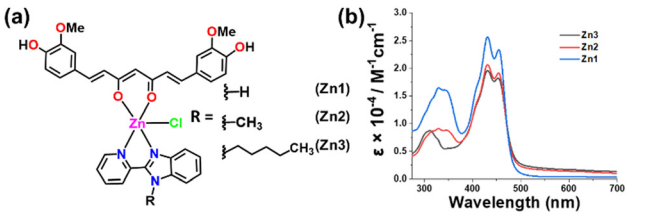

Fig. 1 (a) Chemical structures of **Zn1–Zn3**. (b) UV-Vis spectra of **Zn1–Zn3** in DMSO : water (1 : 9 v : v) solution.

[a] *Department of Chemistry, Indian Institute of Technology (BHU), Varanasi, Uttar Pradesh 221005, India. E-mail: samya.chy@itbhu.ac.in*
[b] *School of Biomedical Engineering, Indian Institute of Technology (BHU), Varanasi, Uttar Pradesh 221005, India. E-mail: sudip.bme@iitbhu.ac.in*
[c] *Division of Organic Chemistry, CSIR-National Chemical Laboratory, Pune 411008, India*

† Electronic supplementary information (ESI) available. See DOI: https://doi.org/10.1039/d5cc02340h

‡ These authors contributed equally to this work.

ensured >97% purity (Fig. S11–S13, ESI†). The UV-Vis spectra of **Zn1–Zn3** showed a strong curcumin-based absorption near 430 nm (Fig. 1b), indicating their potential to sense visible light for antibacterial responses.[11] **Zn1–Zn3** displayed a curcumin-based emission maximum at *ca.* 545 nm (λ_{ex} = 430 nm) (Fig. S14, ESI†).[11] The octanol–water partition coefficients ($\log P_{o/w}$ value) of **Zn1–Zn3** were *ca.* +1.6 to +2.5, indicating their lipophilic characteristics. **Zn1–Zn3** showed excellent photostability under light exposure, with no notable spectral changes up to 1 h in DMSO : water (1 : 9, v/v) (Fig. S15, ESI†).

DFT calculations were performed on **Zn1–Zn3** to rationalize their electronic structures and photophysical properties. The optimized structures of **Zn1–Zn3** showed a distorted square pyramidal structure (Fig. 2a and Fig. S16, ESI†). Furthermore, the electronic structures were characterized based on their FMOs (Fig. S17, ESI†). The analysis of the FMOs revealed that the HOMO−1 was localized on the Zn(II) center and Cl. The HOMO and LUMO+1 were distributed on curcumin with slight involvement of Cl. The LUMO was on the benzimidazole moieties. The $E_g = E_{LUMO} - E_{HOMO}$ remained similar for **Zn1–Zn3** (Table S1 and Fig. S18a, ESI†). The calculated UV-Vis spectra of **Zn1–Zn3** were found to be in accordance with the experimental data (Fig. S18b, ESI†). SOMO plots and spin density plots at the triplet excited state of **Zn1–Zn3** (Fig. 2b and Fig. S19, S20, ESI†) revealed that the unpaired electrons are localized on the curcumin mainly.

The absorbance within the visible range and high photostability of **Zn1–Zn3** inspired us to investigate them as aPDT agents. In aPDT, $^1O_2$ production plays a critical role in causing oxidative stress, disrupting membranes, denaturing proteins, and damaging DNA.[4,5] The $^1O_2$ generation ability of **Zn1–Zn3** was determined using diphenyl isobenzofuran (DPBF) as a $^1O_2$ probe.[12] The absorbance of DPBF remained unchanged in the presence of **Zn1–Zn3** (Fig. S21, ESI†) under dark conditions, indicating no detectable $^1O_2$ generation. However, there was a gradual decrease in the DPBF-based absorption peaks when light was exposed, exhibiting light-triggered $^1O_2$ generation (Fig. S22, ESI†). The $^1O_2$ quantum yield (Φ_Δ) of **Zn1–Zn3** was 0.07–0.11 with $[Ru(bpy)_3]Cl_2$ as standard (Φ_Δ = 0.22) (Fig. 2c and Fig. S23, ESI†).[12] To gain insight into the underlying PDT mechanism, we further investigated the excited singlet/triplet state properties of **Zn3** (Tables S2 and S3, ESI†). The obtained result revealed several triplet states with higher energy than 0.98 eV, the energy required to convert cellular $^3O_2$ into reactive $^1O_2$ (Table S3, ESI†).[13] Usually, the intersystem crossing (ISC) efficiently occurs when there is a small energy gap ($\Delta E_{S_1-T_n} < 0.3$ eV) between the S_1 and T_n states.[13] Thus, based on excitation energy analysis, the possible channels for ISC transitions of **Zn3** are given in Fig. 2d. The NTO analysis of these transitions indicated the involvement of ^{1}LLCT to ^{3}LLCT transitions (Fig. 2e and Fig. S24, ESI†). It is essential to mention that Zn(II) complexes possess a d^{10} configuration that restricts the excited states' internal quenching by low-lying d–d* states.[13] Thus, low-cost and biocompatible Zn(II) complexes might be attractive aPDT agents.

Molecular docking (MD) has emerged as a powerful tool for identifying the therapeutic role of drugs in their antibacterial activity. We performed molecular docking with **Zn1–Zn3** and three crucial target proteins, such as TasA (PDB ID: 5OF2) of gram-positive (*B. subtilis*) and PgaB (PDB ID: 4P7O) and FabH (PDB ID: 1EBL) of gram-negative (*E. coli*) bacteria (Fig. 2f–h and Fig. S25, ESI†).[14] TasA is a major structural protein in the biofilms of *B. subtilis*, contributing to stability and resilience.[14] PgaB plays a crucial role in the biofilm formation process by deacetylating poly-β-1,6-*N*-acetyl-D-glucosamine.[14] FabH is a key enzyme in bacterial fatty acid biosynthesis, essential for cell membrane formation. Its inhibition can disrupt lipid metabolism.[14] Thus, the complexes

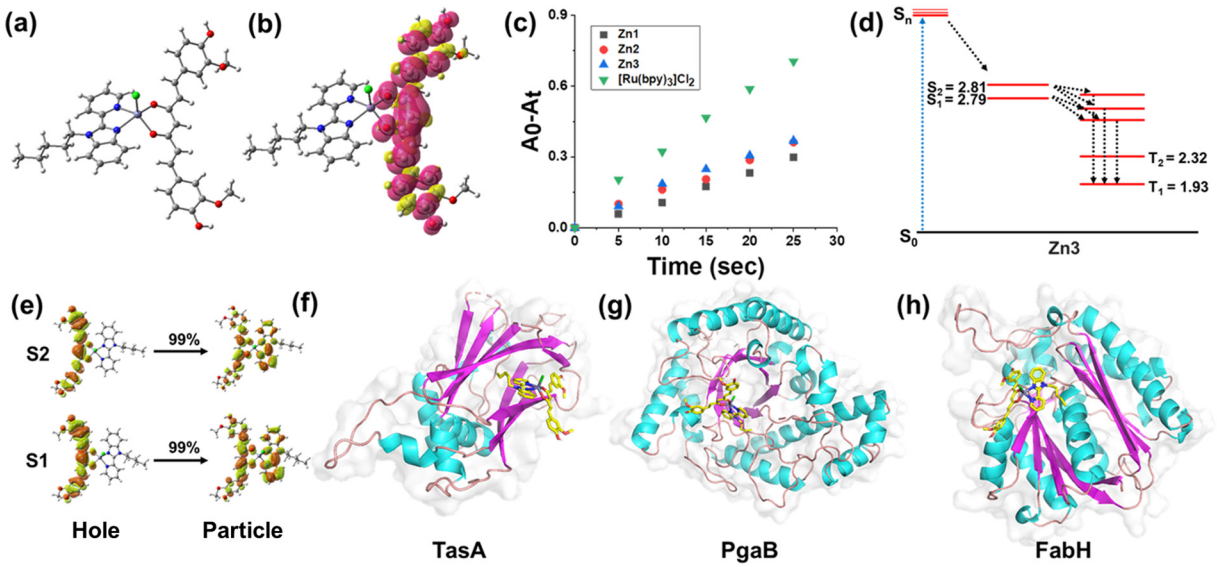

Fig. 2 (a) Optimized structure of **Zn3**. (b) Spin density distribution on **Zn3** at the adiabatic triplet state. (c) $^1O_2$ generation by **Zn1–Zn3** (5 μM) with respect to time in DMSO : water (2 : 98 v : v) solution. (d) Calculated excited state energy and possible ISC channels of **Zn3** (energy in eV). (e) NTOs for $S_0 \rightarrow S_1/S_2$ transition for **Zn3**. (e)–(h) Domain architecture of the **Zn3**-docked structure with (f) TasA; (g) PgaB; and (h) FabH.

displaying favourable binding interactions against these crucial proteins may show promising antibacterial and antibiofilm activity. The MD result of **Zn1–Zn3** with these target proteins underlined their notable binding interactions with the key amino acids *via* hydrogen bonding, pi interaction, van der Waals interaction, *etc.* (Fig. S26–28, ESI†). The docking results are summarized in Table S4, ESI.† Against PgaB and TasA, **Zn3** exhibited higher binding efficacy than **Zn1** and **Zn2** due to more H-bonding. In the case of FabH, **Zn1** showed better binding efficacy than **Zn2** and **Zn3**. The interactions of **Zn1–Zn3** with different receptor surfaces of these proteins are depicted in Fig. S29–S37, ESI.† Overall, **Zn1–Zn3** exhibited notable binding affinities (-8.61 kcal mol^{-1}) and favourable interactions with these key bacterial proteins, surpassing the accepted threshold (-6.0 kcal mol^{-1}) for drug-like binding in docking studies, suggesting their potential antibacterial and antibiofilm effects.[15]

The encouraging visible light-triggered $^1O_2$ generation ability and molecular docking results of **Zn1–Zn3** pushed us to determine their light-activated antibacterial properties against *E. coli* and *B. subtilis*. The time-dependent growth-inhibition kinetics of **Zn1–Zn3** against *E. coli* and *B. subtilis* indicated that **Zn3** significantly inhibited the bacterial growth at 25 μM and 50 μM up to 24 h under light exposure (400–700 nm, 10 J cm^{-2}) (Fig. 3a, b and Fig. S38, ESI†). In the dark, **Zn1–Zn3** showed no inhibition of bacterial growth. Preliminary screening studies revealed that **Zn1** and **Zn2** did not show comparable antibacterial efficacy to **Zn3**. Hence, **Zn3** was selected for further *in vitro* and *in vivo* antibacterial studies.

Zn3 showed minimum inhibitory concentration value, *i.e.*, MIC_{90} = 21.89 μM in *E. coli* and MIC_{90} = 45.5 μM in *B. subtilis* (Fig. S39 ESI†). In a zone inhibition study, upon light irradiation, **Zn3** demonstrated a larger bacterial zone inhibition against *E. coli* (at 25 μM, 50 mm, and at 50 μM, 50 mm) and *B. subtilis* (at 25 μM, 23 mm and at 50 μM, 27 mm) (Fig. S40, ESI†). However, in the dark, **Zn3** showed no bacterial zone inhibition at 25 μM and 50 μM (Fig. S40, ESI†). Moreover, Fig. S41a and b ESI† shows that **Zn3** inhibited *E. coli* and *B. subtilis* colony formation under light exposure compared to the dark.

DCFH-DA assay assessed in-cell ROS generation by **Zn3**, where nonfluorescent DCFH-DA was converted to green-emissive DCF upon reacting with ROS.[12] The obtained result, shown in Fig. 3c and d, revealed that the green fluorescence intensity in the **Zn3** (50 μM) + light-treated groups was found to be 2- to 3-fold higher than under dark conditions in both *E. coli* and *B. subtilis* (Fig. 3c and d). This result revealed that **Zn3** induced significantly higher ROS within bacteria than the control and positive control groups under light exposure.

As a defense strategy against antimicrobial agents, pathogenic bacteria frequently develop biofilms.[15] To validate antibiofilm efficacy, **Zn3** was coated on polydimethylsiloxane (PDMS) disks (used in medical devices and biomedical applications), and the biofilm formation was evaluated using crystal violet staining.[16] **Zn3**-coated PDMS exhibited the strongest biofilm inhibition under light treatment compared to untreated controls and the positive control group, including the dark conditions (Fig. 4a). FE-SEM was used to verify the morphological change of *E. coli* biofilms under both treatment conditions. As shown in Fig. 4b and Fig. S42 ESI,† the control group under dark and light conditions demonstrated the best integrity of the bacterial membrane with a higher number of closely attached bacteria, forming an intact biofilm. However, **Zn3** coating under dark and light conditions drastically reduced total bacterial attachment, causing severe rupture on the surface of the bacterial wall with a notable area of shrinkage. The effect of **Zn3** on the destruction of

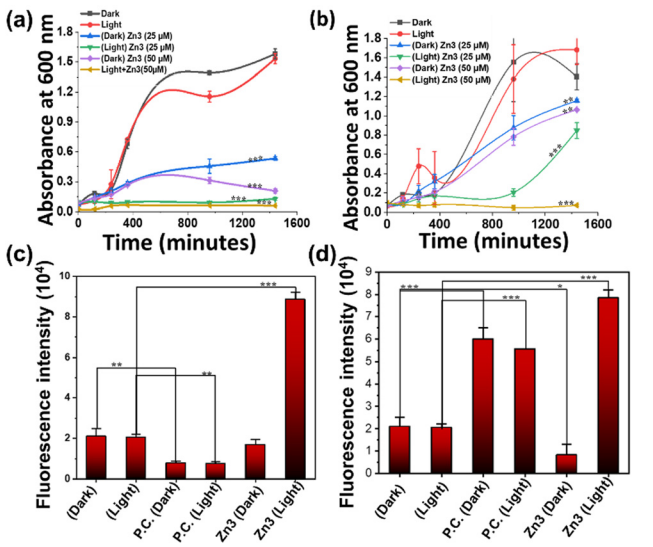

Fig. 3 (a) and (b) Kinetics growth curve of Zn3-treated *E. coli* (a) and *B. subtilis* (b) under light and dark conditions. (c) and (d) In-cell ROS production in (c) *E. coli* and (d) *B. subtilis* induced by **Zn3** (50 μM) under light and dark conditions.

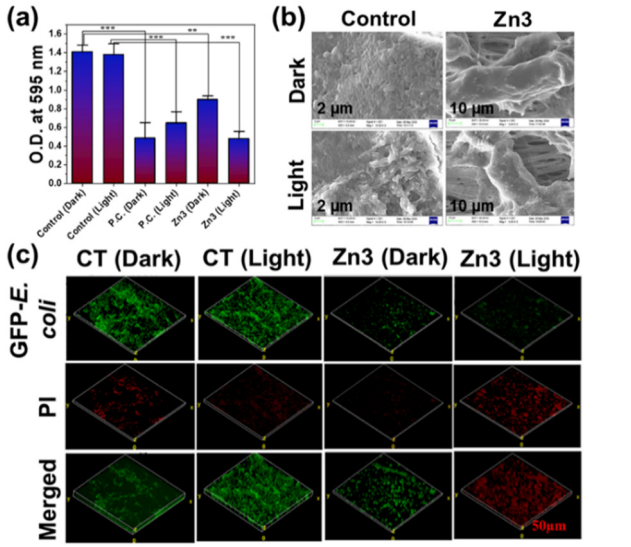

Fig. 4 (a) CV staining assay to quantify the antibiofilm activity of **Zn3**-coated PDMS disks treated with *E. coli*. (b) SEM images of **Zn3**-coated and uncoated PDMS disks (control) incubated with *E. coli* for biofilm formation; scale bar: CT = 2 μm, **Zn3** = 10 μm. (c) Confocal images of the **Zn3**-dark and light-treated group of *E. coli*, CT = control, scale bar: 50 μm.

biofilms was also investigated using confocal laser scanning microscopy. The **Zn3**-coated group effectively eliminated an *E. coli* biofilm under light exposure, similar to the ciprofloxacin (positive control) group (Fig. 4c and Fig. S43, ESI†). In contrast, the uncoated and dark groups showed no such reduction in biofilms. Quantification using ImageJ software revealed a higher number of GFP-*E. coli* in the control group compared to the positive control (P.C.) and **Zn3**-light-treated groups (Fig. S43, ESI†). The fluorescence intensity of dead cells was significantly higher in both the positive control and **Zn3**-light-treated groups (Fig. S43, ESI†). In addition, EPS (extracellular polymeric substances) weight studies also suggested that the **Zn3** under light exposure can inhibit the EPS formation (Fig. S44, ESI†). These findings suggested that **Zn3** effectively destroyed biofilm formation under light irradiation.

Bacterial skin infections caused by *E. coli* are a leading cause of concern in healthcare.[17] These infections vary from mild to more severe illnesses, and the development of AMR for several strains of *E. coli* makes it challenging to treat the infection.[16] The effect of **Zn3** for eradicating bacterial infections was studied in a rat model (Fig. S45, ESI†) by applying **Zn3** (50 μM) on the infected skin under light exposure. The images of the colony plates showed that the treatment with **Zn3+Light**, or ciprofloxacin (P.C.), significantly reduces bacterial colonies compared to the untreated groups at day 3 (Fig. S45, ESI†). However, **Zn3** treatment in the dark did not inhibit the bacterial colonies. Cytotoxicity and haemolysis evaluation of any antibacterial drug is a crucial step to ensure its safety for therapeutic applications.[18] An MTT assay was used to evaluate the toxicity of **Zn3** in HEK-293 (human embryonic kidney) cells. The results revealed that *ca.* 80% of cells were viable at 50 μM (Fig. S46, ESI†), indicating that this dose of **Zn3** is safe for biomedical applications. The haemolysis study of **Zn3** displayed insignificant haemolysis (<5%) in the red blood cells of Wistar rats, ensuring its high biosafety (Fig. S47, ESI†). It is important to highlight that zinc and zinc-associated complexes are biocompatible. In addition, many reports have demonstrated the faster metabolism and degradation of zinc complexes in cellular conditions, with adequate systematic excretion, reducing the risk of long-term toxicity.[19]

In this work, three novel curcumin-based Zn(II)-metallophotoantibiotics, **Zn1–Zn3**, were developed and screened as aPDT agents. *In silico* studies revealed the potential of **Zn1–Zn3** for $^1O_2$ generation and high binding efficacy with crucial target bacterial proteins such as FabH, PgaB of gram-negative (*E. coli*) and TasA of gram-positive (*B. subtilis*) bacteria. **Zn3**, the most active one, eliminated *E. coli* infection in a rat model after visible light activation, while showing good biosafety characteristics. This work expands the scope of Zn(II)-curcumin photoantibiotics development for efficient antibiofilm eradication and *in vivo* bacterial infection treatment. Ongoing efforts are directed to developing red light-sensitive Zn(II)-complexes with enhanced ISC, and potent antibacterial activity, similar to highly active heavy-metal or porphyrin-based aPDT agents. Compared to other photoactive metal complexes such as Ru, Au, Pt, Os, Fe *etc.*, Zn-complexes stand out due to the inherent anti-microbial properties of zinc ions. Moreover, the developing antibacterial Zn-complexes might be a more cost-effective option.

This work was supported by the SERB (now ANRF), India (SRG/2022/000030) and (BT/PR49530/MED/32/839/2023) from DBT, India. R. K. thanks the GOI for the PMRF.

Conflicts of interest

There are no conflicts to declare.

Data availability

The data supporting this article have been included as part of the ESI†

References

1 S. K. Ahmed, S. Hussein, K. Qurbani, R. H. Ibrahim, A. Fareeq, K. A. Mahmood and M. G. Mohamed, *J. Med. Surg. Public Health*, 2024, **2**, 100081.
2 G. Muteeb, M. T. Rehman, M. Shahwan and M. Aatif, *Pharmaceuticals*, 2023, **16**, 1615.
3 A. Frei, A. D. Verderosa, A. G. Elliott, J. Zuegg and M. A. T. Blaskovich, *Nat. Rev. Chem.*, 2023, **7**, 202–224.
4 M. Piksa, C. Lian, I. C. Samuel, K. J. Pawlik, I. D. W. Samuel and K. Matczyszyn, *Chem. Soc. Rev.*, 2023, **52**, 1697–1722.
5 T. W. Rees, P.-Y. Ho and J. Hess, *ChemBioChem*, 2023, **24**, e202200796.
6 X. Hu, H. Zhang, Y. Wang, B.-C. Shiu, J.-H. Lin, S. Zhang, C.-W. Lou and T.-T. Li, *Chem. Eng. J.*, 2022, **450**, 138129.
7 A. Frei, J. Zuegg, A. G. Elliott, M. Baker, S. Braese, C. Brown, F. Chen, C. G. Dowson, G. Dujardin, N. Jung, A. P. King, A. M. Mansour, M. Massi, J. Moat, H. A. Mohamed, A. K. Renfrew, P. J. Rutledge, P. J. Sadler, M. H. Todd, C. E. Willans, J. J. Wilson, M. A. Cooper and M. A. T. Blaskovich, *Chem. Sci.*, 2020, **11**, 2627–2639.
8 C. Wegeberg and O. S. Wenger, *JACS Au*, 2021, **1**, 1860–1876.
9 J. P. McClung and A. G. Scrimgeour, *Mil. Med.*, 2005, **170**, 1048–1052.
10 T. H. S. Souza, J. F. Sarmento-Neto, S. O. Souza, B. L. Raposo, B. P. Silva, C. P. F. Borges, B. S. Santos, P. E. C. Filho, J. S. Reboucas and A. Fontes, *J. Photochem. Photobiol., C*, 2021, **49**, 100454.
11 S. Banerjee and A. R. Chakravarty, *Acc. Chem. Res.*, 2015, **48**, 2075–2083.
12 (*a*) E. Vitaku, D. T. Smith and J. T. Njardarson, *J. Med. Chem.*, 2014, **57**, 10257–10274; (*b*) L. Wanka, K. Iqbal and P. R. Schreiner, *Chem. Rev.*, 2013, **113**, 3516–3604.
13 (*a*) R. Kushwaha, V. Singh, S. Peters, A. K. Yadav, D. Dolui, S. Saha, S. Sarkar, A. Dutta, B. Koch, T. Sadhukhan and S. Banerjee, *J. Phys. Chem. B*, 2023, **127**, 10266–10278; (*b*) G. Xu, C. Li, C. Chi, L. Wu, Y. Sun, J. Zhao, X.-H. Xia and S. Gou, *Nat. Commun.*, 2022, **13**, 3064.
14 (*a*) X. Lu, J. Tang, Z. Zhang and K. Ding, *Curr. Med. Chem.*, 2015, **22**, 651–667; (*b*) X. Wang, J. F. Preston and T. Romeo, *J. Bacteriol.*, 2004, **186**, 2724–2734; (*c*) D. Romero, C. Aguilar, R. Losick and R. Kolter, *Proc. Natl. Acad. Sci. U. S. A.*, 2010, **107**, 2230–2234.
15 (*a*) M. García-Ortegón, G. N. C. Simm, A. J. Tripp, J. M. Hernández-Lobato, A. Bender and S. Bacallado, *J. Chem. Inf. Model.*, 2022, **62**, 3486–3502; (*b*) L. Ivanova and M. Karelson, *Molecules*, 2022, **27**, 9041.
16 (*a*) P. D. Martino, *AIMS Microbiol.*, 2018, **4**, 274–288; (*b*) I. Miranda, A. Souza, P. Sousa, J. Ribeiro, E. M. S. Castanheira, R. Lima and G. Minas, *J. Funct. Biomater.*, 2021, **13**, 2.
17 M. Croxen and B. Finlay, *Nat. Rev. Microbiol.*, 2010, **8**, 26–38.
18 I. Bacskay, D. Nemes, F. Fenyvesi, J. Varadi, G. Vasvari, P. Feher, M. Vecsernyes and Z. Ujhelyi, *Cytotoxicity*, 2017, 978-1-78923-431-2.
19 B. Chen, P. Yu, W. N. Chan, F. Xie, Y. Zhang, L. Liang, K. T. Leung, K. W. Lo, J. Yu, G. M. K. Tse, W. Kang and K. F. To, *Signal Transduction Targeted Ther.*, 2024, **9**, 6.

